DYNAMICALLY PROPAGATING SHEAR BANDS IN IMPACT-LOADED PRENOTCHED PLATES—I. EXPERIMENTAL INVESTIGATIONS OF TEMPERATURE SIGNATURES AND PROPAGATION SPEED

M. ZHOU,† A. J. ROSAKIS‡ and G. RAVICHANDRAN‡

† George W. Woodruff School of Mechanical Engineering, Georgia Institute of Technology, Atlanta, GA 30332-0405, U.S.A.; and ‡Graduate Aeronautical Laboratories, California Institute of Technology, Pasadena, CA 91125, U.S.A.

ABSTRACT

The initiation and propagation of shear bands are investigated by subjecting prenotched plates to asymmetric impact loading (dynamic mode-II). The materials studied are C-300 (a maraging steel) and Ti–6Al–4V. A shear band emanates from the notch tip and propagates rapidly in a direction nearly parallel to the direction of impact. When the impact velocity is higher than a critical value, the shear band propagates throughout the specimen. The shear band arrests inside the specimen when the impact velocity is below this critical value. In the latter case and for the C-300 steel, a crack initiates and propagates from the tip of the arrested shear band at an angle to the direction of shear band propagation. Microscopic examinations of the shear band and crack surfaces reveal a ductile mode of shear failure inside the shear band and an opening mode of failure for the crack. The coexistence of shear banding and fracture events in the same specimen signifies a transition in the modes of failure for this material under the conditions described. For Ti–6Al–4V, the only mode of failure observed is shear banding. While the transition is induced by changes in loading conditions, the different behaviors of these two materials suggest it is also related to material properties. The experimental investigation focuses on both the thermal and the mechanical aspects of the propagation of shear bands. Real time temperature histories along lines intersecting and perpendicular to and along the shear band path are recorded by means of a high speed infrared detector system. Experiments show that the peak temperatures inside the propagating shear bands increase with impact velocity. The highest temperature measured is in excess of 1400°C or approximately 90% of the melting point of the C-300 steel. For Ti–6Al–4V, the peak temperatures are approximately 450°C. In the mechanical part of the study, high speed photography is used to record the initiation and propagation of shear bands. Recorded images of propagating shear bands at different impact velocities provide histories of the speed of shear band propagation for the C-300 steel. A strong dependence of shear band speed on the impact velocity is found. The highest speed observed for the C-300 steel is approximately 1200 ms^{-1} or 40% of its shear wave speed. Copyright © 1996 Elsevier Science Ltd

1. INTRODUCTION

The localization of deformation into narrow bands of high rates of straining and intense heating plays an important role in many applications involving structural materials. Issues related to the formation of such bands include structural integrity in vehicle crash-worthiness, product quality and efficiency in high speed machining and

981

high speed forming and improvement of performance in armor penetration. Because of its importance, this phenomenon has received significant attention in the open literature, e.g. Recht (1964), Rogers (1979), Clifton (1980), Bai (1981, 1982), Rogers and Shastry (1981), Merzer (1982), Freund *et al.* (1985), Molinari and Clifton (1987), Wright and Walter (1987), Giovanola (1988), Shawki and Clifton (1989), Duffy and Chi (1992), Batra and Kim (1992), Zbib and Aifantis (1992), Shawki (1992), Zhou *et al.* (1994), and Zurek (1994). There is now a better understanding of the roles of many factors in the formation of shear bands, including mechanical and thermal properties and microstructural variations. Most of the available literature considers shear bands to be one-dimensional entities. However, shear bands in most applications are often two- or three-dimensional entities, and like propagating cracks, are an important form of failure. The two-dimensional nature of these problems assigns them attributes that are not normally present in one-dimensional shear band models. These characteristics include a dynamically propagating tip, and thus the dependence of thermal and mechanical fields on the speed of propagation. Because different materials exhibit different resistances to the propagation of shear bands, a wide range of thermal and mechanical behaviors may exist. Such differences are demonstrated by temperature and deformation fields around the propagating bands and their strong dependence on propagation speeds. Relatively little information is available on the dynamic extension of these shear bands. Using high speed photography, Marchand and Duffy (1988) observed the non-uniform initiation and propagation of shear bands in thin-walled tubular specimens subjected to dynamic torsional loading. They also reported an estimated shear band tip speed of approximately 500 ms^{-1}. The initiation of shear bands was studied by Needleman (1989) under a two-dimensional framework. Grady (1992) analyzed the characteristics of propagating shear bands based on the results of a one-dimensional approximate model. The structure of propagating shear bands was analyzed recently by Gioia and Ortiz (1996). To study this class of shear bands, an experimental configuration that provides controlled shear band initiation and propagation is needed. Since this problem involves strong coupling between the thermal and mechanical processes of dynamic deformation, an ideal configuration should allow both processes to be investigated.

  Kalthoff (1987) and Kalthoff and Winkler (1987) studied the propagation of shear bands using double-notched plates impacted by a cylindrical projectile. For each notch the impact is asymmetric. The initiation of shear bands from the notch tips is facilitated by intense shearing in their vicinities. This configuration provides an opportunity to study shear band initiation and propagation under well-controlled conditions. In this experiment, shear banding is actually only one of the failure modes observed. Kalthoff and Wrinkler (1987) also reported a brittle-to-ductile transition of failure mode in a maraging steel. At low impact velocities, a crack extends in a direction approximately 70° from the direction of impact. Lee and Freund (1990), using an elastodynamic analysis, showed that this angle coincides with the direction of the maximum circumferential tensile stress in the K^{d}-dominant field at the notch tip. When the impact velocity is raised to above a critical value a shear band emanates from the notch tip in a direction nearly parallel to the direction of impact. Needleman and Tvergaard (1994), using a finite element analysis, attributed this transition to the fact that at higher loading rates increased plastic strain and thermal softening reduce

the maximum tensile stress in the specimen and therefore can effectively suppress the brittle failure observed at lower loading rates.

Mason *et al.* (1994a) conducted similar experiments on C-300, a high strength maraging steel. Their goal was to investigate the nature of the deformation fields at the vicinity of propagating shear bands in real time. The specimen configuration differs from that used by Kalthoff (1987) and Kalthoff and Wrinkler (1987) in that it contains only one notch instead of two. This difference allows the notch tip to be loaded for a longer duration by the incoming pulse without the effects of diffracted waves from a neighboring notch. A transition of failure mode in the form of shear banding followed by fracture was also observed. In addition, they reported deformation patterns around a shear band recorded by the coherent gradient sensor (CGS) and high speed photography. By comparing the interferograms with the deformation fields predicted by a mode-II Dugdale model they obtained estimates for the shear stress histories inside the shear band, the stress intensity factor at band initiation and the time history of shear band length.

In the current study, experiments were conducted on C-300 and Ti–6Al–4V using the configuration of Mason *et al.* (1994a). This configuration is chosen because the location and direction of band initiation and propagation are known, therefore allowing accurate thermal and mechanical measurements to be made. The objective is to understand the conditions under which shear bands initiate and propagate and to investigate and characterize the transition in the mode of failure between shear bands and cracks. Our approach is to study both the thermal and the mechanical processes during shear band initiation and propagation. The study of the thermal process is important since dynamic shear banding is primarily driven by thermal softening due to heat generated by plastic deformation. The mechanical study allows us to record the propagation of the shear bands and the transition of failure mode. This combined thermal and mechanical approach involves the use of both high speed optical and infrared diagnostics in the experiments. The thermal part of the experimental study uses a high speed infrared InSb (indium antimonide) detector array to obtain the temperature fields around the propagating shear bands. In this paper, primary attention is given to the process of the propagation of shear bands. Specifically, high speed photography is used to study the time of initiation, the shear band speed histories and their dependence on impact velocity. The optical images also provide evidence for the failure mode transition following the arrest of the shear band.

The present investigation is a combined experimental and computational effort. Finite element simulations using the actual experimental conditions and independently measured material properties are conducted in parallel to the experiments. The simulations are full-scale calculations that account for full thermo-mechanical coupling in the field equations of dynamic deformation. The material is considered to be an elastic–viscoplastic solid and finite kinematics are used. Such a combined experimental and numerical approach enables us to identify the factors that play important roles in the initiation and propagation of the shear bands. Furthermore, it allows us to analyze the process that leads to the selection of failure modes at different loading rates under the actual conditions of the experiments. In this paper, which is the first part of a two-part series, we present the results of our experiments. In the second part (Zhou *et al.*, 1996), results of the numerical simulations are discussed.
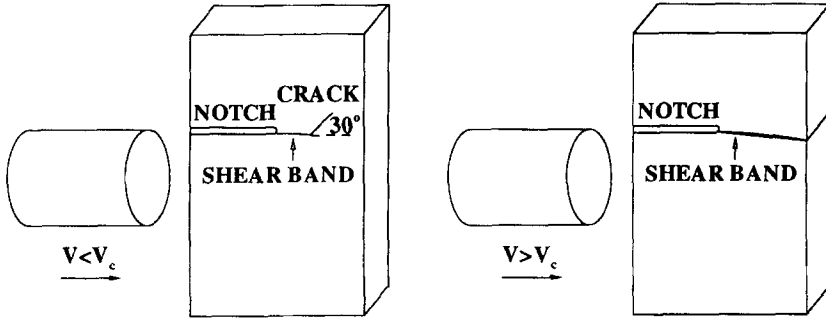
M. ZHOU *et al.*

Fig. 1. Asymmetric impact configuration and failure modes.

2. DESCRIPTION OF FAILURE MODES

Figure 1 is a schematic of the asymmetric impact configuration used in the experiments. The specimen is a rectangular plate with a notch. During the experiment, the specimen is impacted by a cylindrical projectile 50.8 mm (2 inches) in diameter and 76.2 mm (3 inches) in length on one side of the notch. A mode-II type of loading is achieved when dilatational stress waves generated by the impact arrive at the notch tip. A schematic drawing of the specimen geometry and dimensions is shown in Fig. 2. The rectangular specimen is 203.2 mm (8 inches) in length, 101.6 mm (4 inches) in width and 6.35 mm (0.25 inch) in thickness. The notch, approximately 300 μm in width, is pre-machined into the specimen by electric discharge machining (EDM). Two materials are used in the experiments, C-300 (a high strength maraging steel)
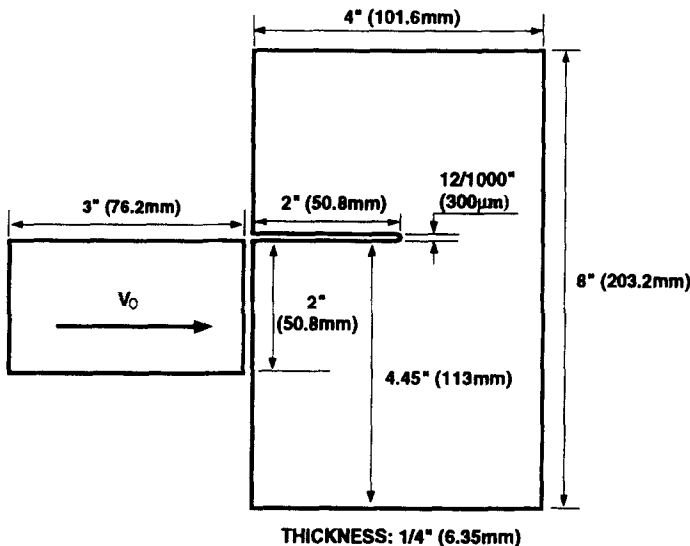

Fig. 2. Dimensions of the specimen used in the asymmetric impact experiment.

and Ti–6Al–4V (a titanium alloy). These materials possess different combinations of mechanical and thermal properties which may greatly influence their resistance to shear banding.

The observed failure modes are qualitatively illustrated in Fig. 1. A shear band initiates from the notch tip when the impact velocity V_0 is greater than approximately 20 ms^{-1} for the C-300 steel. The shear band propagates in a direction nearly parallel to the direction of impact. When V_0 is also below approximately 29 ms^{-1}, the band eventually arrests within the specimen and a dynamic crack extends from the tip of the arrested shear band in a direction approximately 30° to the direction of impact [Fig. 1(a)]. When V_0 is greater than 29 ms^{-1}, the shear band propagates throughout the whole ligament and no crack is observed [Fig. 1(b)].

Figure 3 shows photographs of C-300 specimens exhibiting both failure modes after impact. The impact velocity is approximately 23.4 ms^{-1}. The length of the shear bands is 16 mm. Figure 3(a) is a plan view of the shear band and the crack. Figure 3(b) shows the morphologies of the separated failure surfaces. The shear band surface is shiny and smooth, indicating a mode of failure associated with in-plane shear deformation. Shear deformation is uniform over the whole thickness of the specimen indicating a two-dimensional or planar mode of deformation. The crack surface is gray and rough, and appears fibrous. Such characteristics are typical of crack surfaces resulting from tensile failure. The crack surface also shows shear lips, indicating some three-dimensionalities typical of tensile fracture processes. The two different failure mechanisms observed here can be better seen in detailed microscopic examinations of the two failure surfaces. Figure 4(a) is a scanning electron micrograph of the surface of the shear band in Fig. 3(a). The shearing direction is vertical in this picture. The densely populated and elongated voids indicate ductile shear deformation inside the shear band. This micrograph clearly shows that the failure inside the shear band is a direct result of sheared and coalesced voids. The average void size is approximately 10 μm. Note that the morphology of the surface indicates plastic flow similar to the shear flow of a very soft material smeared by the relative motion of the two sides of the shear band. These features signify material softening by very high temperatures inside the shear band (temperatures that are significant fractions of the melting point of the specimen material). Similar observations of sheared voids and extensive smearing have also been reported by Giovanola (1988) in torsional experiments. A scanning electron micrograph of the crack surface in Fig. 3(a) is shown in Fig. 4(b). No elongated voids are seen here. Clearly, the mode of failure associated with this part of the specimen is tensile in nature (coalescence of voids growing in a primarily tensile field of high triaxialities) and does not involve the type of shear deformation observed in Fig. 4(a). This coexistence of a predominantly shear type of failure and an opening type of failure indicates the occurrence of a transition in the mode of failure which may exist in the C-300 steel. Results of numerical simulations presented in Part II of this investigation (Zhou et al., 1996) illustrate that the changes in loading conditions in the specimen are responsible for this transition in the failure mode. While the in-plane shear loading generated by the asymmetric impact causes the initiation and propagation of the shear band, tensile or opening mode of loading that develops due to release waves from boundaries causes the crack to form, as demonstrated by finite element simulations in Part II of this investigation. Figure 5

shows a specimen of C-300 steel with a shear band that has propagated through the whole ligament. The projectile velocity in this experiment is 29.6 ms^{-1}. The shear band path initially follows closely the direction of impact. After propagating for approximately 30 mm, the shear band advances along a path that curves toward the impacted side of the specimen. Here, the absence of a crack is a result of the significantly higher impact speed. Sufficiently high speeds allow the shear band to propagate out of the specimen before tensile loading conditions can develop to cause the tensile mode of failure as seen in Fig. 3. The dependence of shear band speed on impact velocity will be discussed in Section 5 of this paper.

A similar shear mode of failure is observed for the titanium alloy. The micrograph in Fig. 4(c) shows the morphology of the shear band surface of a Ti–6Al–4V specimen. In this micrograph, the average size of the voids is 25–30 μm. The sheared voids are very clearly delineated and unlike in Fig. 4(a) there is no evidence of extensive smearing. This indicates that temperatures inside the band are probably a lower fraction of the melting point than in the case of C-300 steel. Indeed, direct measurements of the temperature fields discussed later in this paper confirm these observations and provide further insight into the dynamic failure behaviors of these two materials. The tensile mode of failure in Fig. 3 is not observed for Ti–6Al–4V.

3. EXPERIMENTAL APPARATUS

Figure 6 is a schematic illustration of the experimental apparatus used in this study. The system allows both the thermal and the mechanical processes associated with the propagation of shear bands to be studied simultaneously using high speed infrared temperature measurements and high speed photography. The impact loading of the specimen is achieved inside the test chamber of a gas gun shown in the middle of the schematic. A projectile is launched through the barrel and impacts the specimen upon exiting the muzzle end, causing the asymmetric loading illustrated in Fig. 1. The projectile velocity is measured using a photodetector mounted at the muzzle end of the gun barrel, by recording the times at which a light beam is interrupted by the two ends of the cylindrical projectile. A strain gauge is mounted on the specimen near the impact face. Upon impact, output generated by the strain gauge is used to trigger the digital oscilloscopes that record the signals from the high speed infrared detectors used to measure the temperatures. The same gauge output also triggers the high speed camera that records images of the propagating shear bands.

The high speed optical observations described here concern the measurement of the shear band length histories. This part of the experimental setup is shown on the right hand side of Fig. 6. An expanded and collimated laser beam is used to illuminate the specimen. The reflected beam is sent into a Cordin model 330 high speed camera which records images of the impacted specimen at framing rates up to 2×10^6 frames per second. A grid of parallel lines with a pitch of approximately 0.7 mm is deposited on the specimen surface before the experiment to assist the visualization of shear band propagation. The length and velocity histories of the propagating shear bands are obtained from the recorded images. The setup for temperature measurement is illustrated on the left side of the gas gun. This technique is designed to record
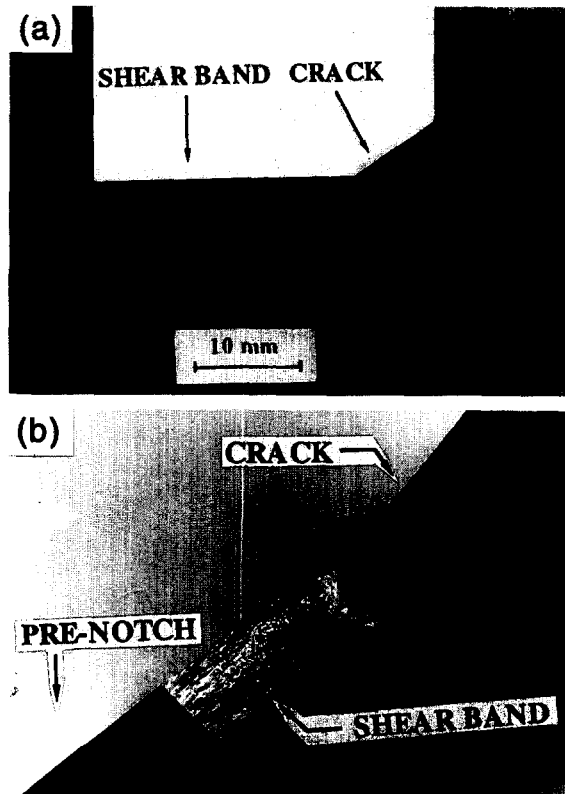
Fig. 3. Failure modes at intermediate impact velocities, $V_0 = 23.4 \text{ ms}^{-1}$, C-300 steel.
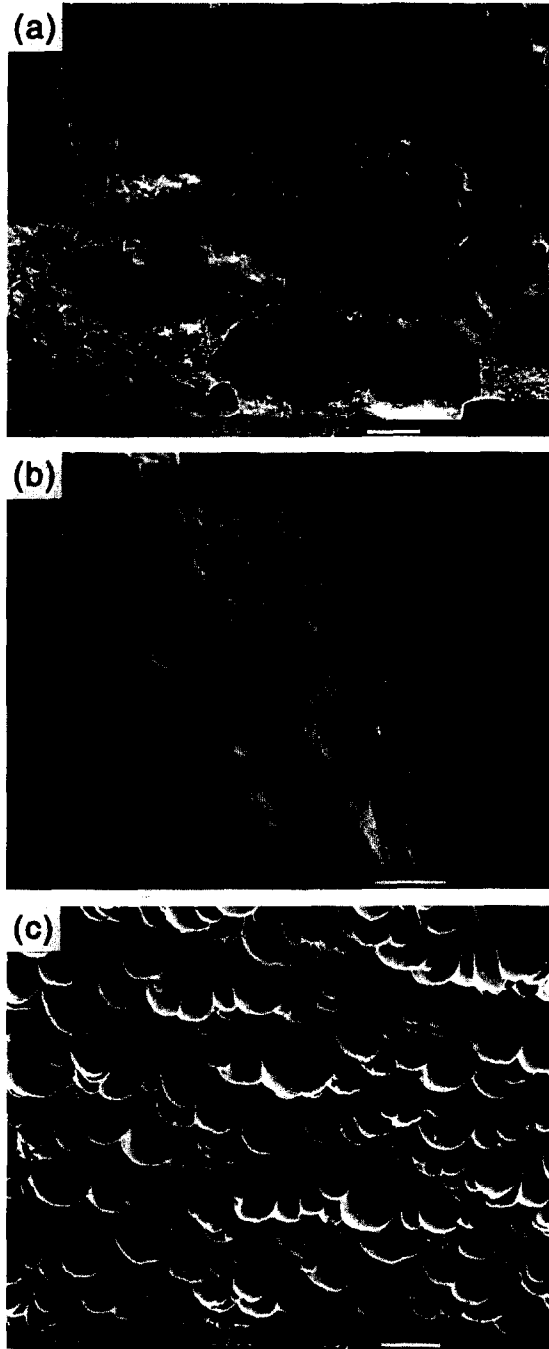
Fig. 4. Shear band and crack surfaces of impacted specimens. (a) Shear band surface (C-300 steel); (b) crack surface (C-300 steel); (c) shear band surface (Ti–6Al–4V).
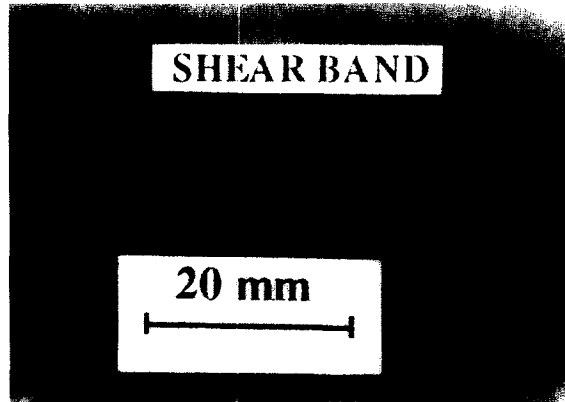
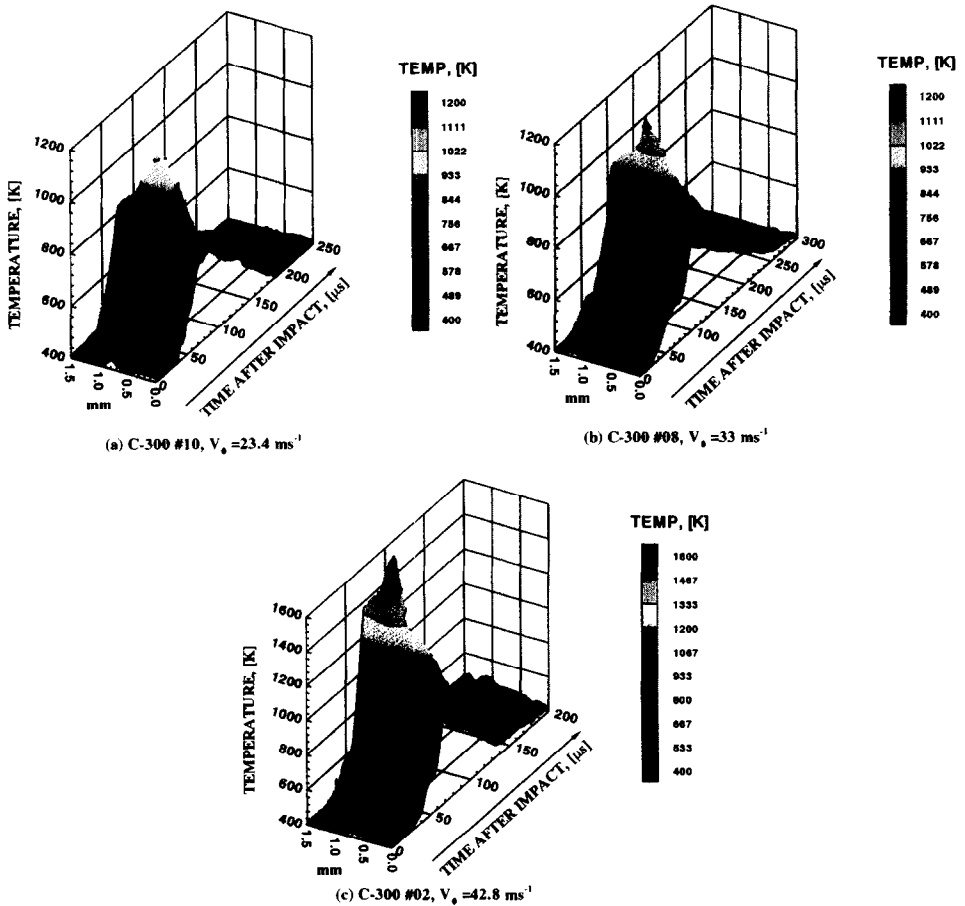Fig. 5. Failure mode at high impact velocities, C-300, $V_0 = 29.6$ ms^{-1}.

(a) C-300 #10, V_s =23.4 ms^{-1}

(b) C-300 #08, V_s =33 ms^{-1}

(c) C-300 #02, V_s =42.8 ms^{-1}

Fig. 9. Temperature profiles around propagating shear bands; C-300 steel. (a) C-300, $V_0 = 23.4$ ms^{-1}; (b) C-300, $V_0 = 33$ ms^{-1}; (c) C-300, $V_0 = 42.8$ ms^{-1}.

M. ZHOU *et al.*
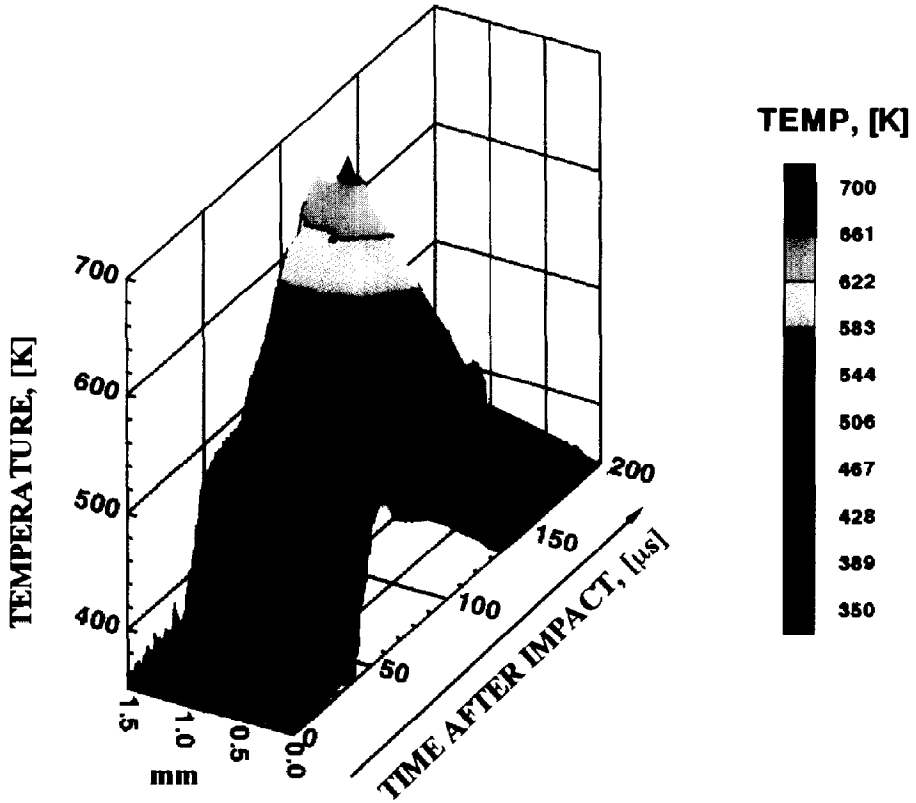
Fig. 11. Temperature profiles around a propagating shear band, Ti–6Al–4V, $V_0 = 47.3\ \text{ms}^{-1}$.

C300, $V_0 = 25$ ms^{-1}, $V_{\mathrm{sb}} = 595$ ms^{-1}

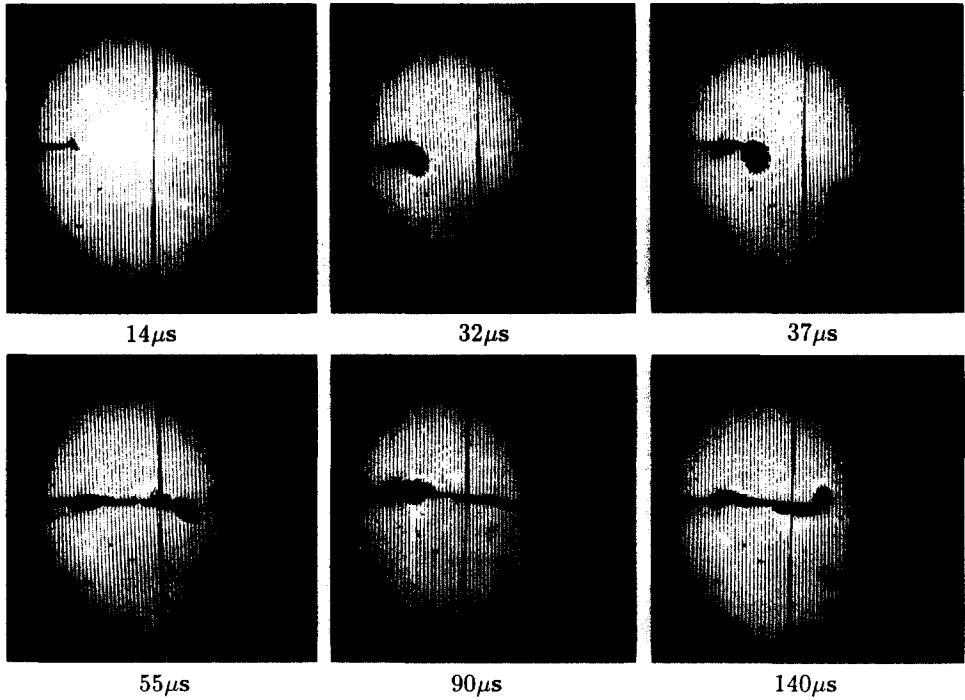
Fig. 16. Images of a propagating shear band and emerging crack recorded by high speed photography, C-300, $V_0 = 25$ ms^{-1}.

M. ZHOU *et al.*

C300, $V_0 = 30 \text{ ms}^{-1}$, $V_{sb} = 1004 \text{ ms}^{-1}$

14μs   39μs   43μs

47μs   51μs   64μs
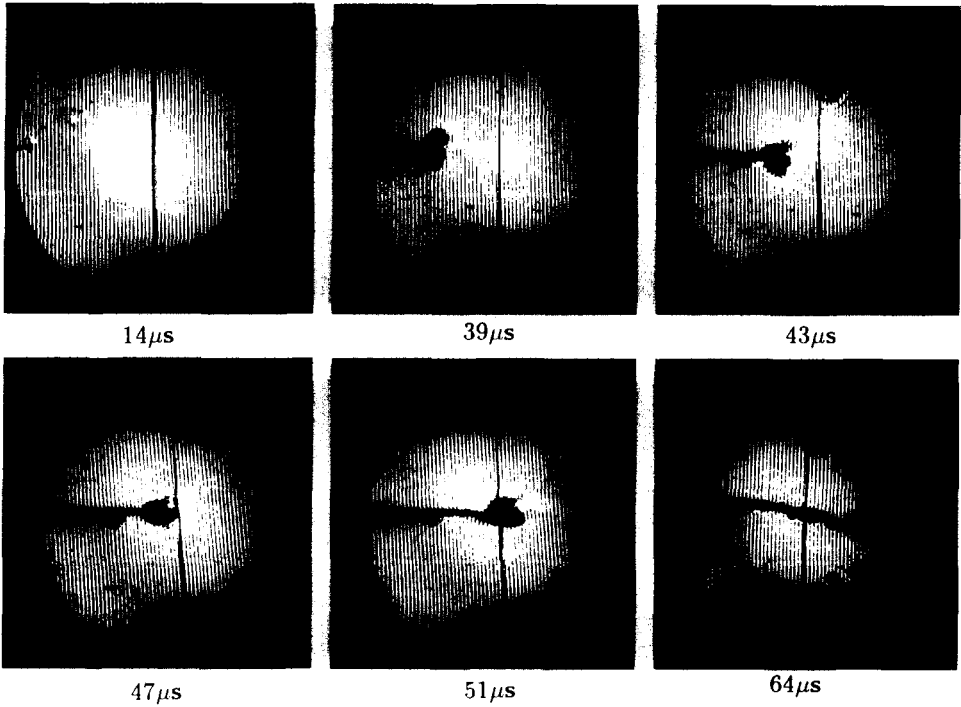
Fig. 17. Images of a propagating shear band recorded by high speed photography for a specimen without a failure mode transition, C-300, $V_0 = 30 \text{ ms}^{-1}$.
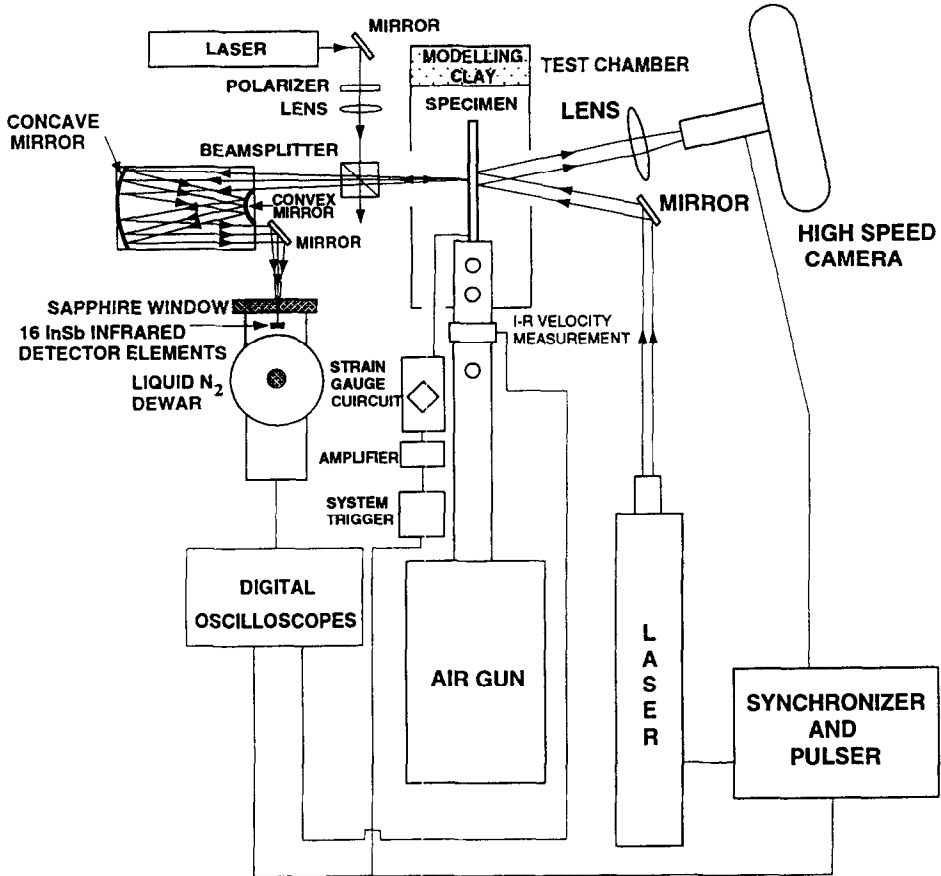
Fig. 6. Experimental apparatus.

temperature histories along a line perpendicular or parallel to the shear band. The measurement makes use of a linear array of infrared detectors. Such a system was described and used by Zehnder and Rosakis (1991, 1992) and Zehnder and Kallivayalil (1991) in studies of temperature rises at the tip of dynamically propagating cracks. This is a non-contact measurement. The detectors, cooled by liquid nitrogen to increase sensitivity and reduce noise, are located away from the specimen, in the image plane of a reflective optical system. The detectors used are high-speed infrared InSb (indium antimonide) detectors with a rise time of approximately 0.5 μs. This response is significantly faster than anticipated temperature increases associated with propagating shear bands. During the experiments the detector signals are recorded by a set of high speed digital oscilloscopes. Temperature profiles around the shear bands are obtained from the recorded detector voltage output through predetermined detector calibration curves. The calibration of the detectors is conducted by correlating the detector output and temperatures of a uniformly heated plate of the same material, thickness and surface finish as the specimen when this plate replaces the specimen in the actual experimental setting. For details on the calibration method, see Zehnder and Rosakis (1992).
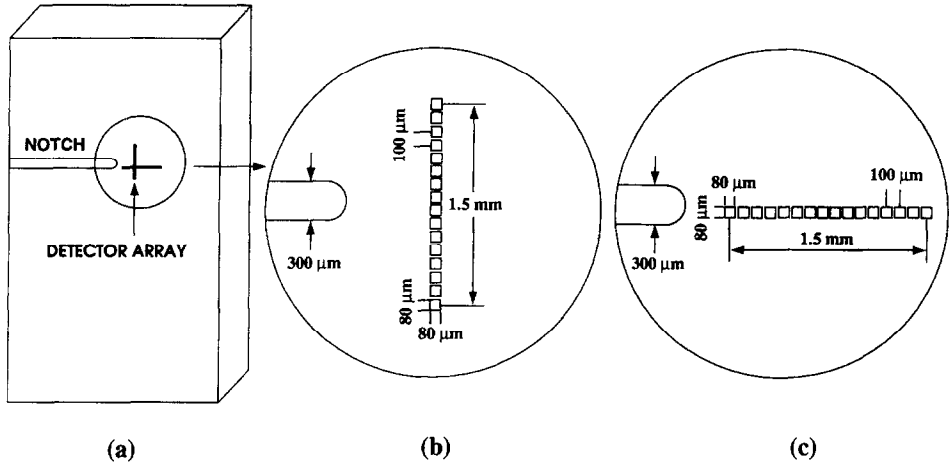
Fig. 7. A schematic illustration of the infrared temperature measurement schemes used in the experiments.

The optical system, which consists of a concave mirror and a convex mirror, has unit magnification. Before each experiment, the specimen, the optical system and the detectors are aligned so that radiation is collected from the precise locations where temperatures are to be measured. Since infrared radiation is invisible, an optical technique, as illustrated in the upper left portion of Fig. 6, is used for the alignment. A laser beam is focused normally, through a beamsplitter, at a point on the specimen surface where temperature is to be measured. The reflected beam is passed through the optical system and focused on to a desired detector element. The polarizer shown is used to reduce the intensity of the laser beam so that damage to the detector elements is avoided. After the optical alignment is completed, the beamsplitter is removed so that infrared radiations can reach the detectors. Final alignment of the detectors involves placing thin wires (200 μm in diameter) on the specimen surface along the exact path whose temperatures are to be measured. An electric current is passed through the wire to increase its temperature, thus allowing infrared radiation from the wire to be used in more accurate alignment between the specimen and the detectors.

The linear array of detectors consists of 16 elements, each being 80 × 80 μm in size. The center-to-center distance between two neighboring elements is 100 μm and the whole array covers a distance of 1.5 mm. The detector array is focused on a line either perpendicular or parallel to the shear band, as illustrated in Fig. 7. When the array is oriented perpendicular to the shear band, as shown in Fig. 7(b), temperature fields around the propagating shear band are obtained as the band propagates toward and passes through the line of observation. In the experiments reported here, this vertical line of observation is located 2–4 mm from the tip of the notch. When the detector array is oriented along the band, as shown in Fig. 7(c), temperature variation along the band can be obtained. Also, this provides an opportunity for the propagation speed of the shear band to be estimated from the time delays in the temperature histories at different points along the shear band path. In the results presented in this

paper, the detector elements are numbered 1 through 16. In Fig. 7(b), element 1 is the lowest element in the array and element 16 is the highest. In Fig. 7(c), element 1 is the left-most element and element 16 is the right-most element.

## 4. TEMPERATURE FIELDS GENERATED BY PROPAGATING SHEAR BANDS

Figure 8(a–c) shows the temperature profiles recorded for C-300 steel specimens tested at impact velocities of 23.4, 33 and 42.8 ms^{-1}, respectively, using the configuration of Fig. 7(b). Each curve represents the temperature history at one point on a line perpendicular to the extending shear band. For these three experiments, the line of observation is located at 3, 3.5 and 2.5 mm in front of the notch tip, respectively. The lowest temperature shown is approximately 410 K instead of the room temperature (293 K). This is because the high speed infrared detectors are only sensitive to radiations at temperatures above 410 K for this material. Below this temperature, detector outputs have the same or lower magnitude than background noise and accurate readings cannot be obtained. As the shear band tips propagate toward and pass through the line of observation, temperatures increase to a maximum in 40–80 μs. Three-dimensional presentations of the data in Fig. 8 are shown in Fig. 9(a–c). The vertical axis represents temperature. The short axis in the horizontal plane represents distance along the line of measurement (direction perpendicular to the propagating band). The long axis in the horizontal plane signifies time after impact. The arrows point to the direction of increasing time. This can also be interpreted as the direction of shear band propagation. The 3-D contour plots reveal the spatial structure of the temperature fields generated by the propagating shear bands. The spikes in the middle indicate the location of the bands. The width of the zone of intense heating is approximately 200–300 μm. It can be seen from Figs 8 and 9 that the maximum temperature increases with impact velocity. When the impact velocity is 42.8 ms^{-1}, the maximum temperature is approximately 1427°C (1700 K). This temperature is approximately 90% of the melting point of the C-300 steel (1570°C). The temperatures reported here are significant fractions of the melting point and are consistent with the smeared zones of deformation observed in the micrograph of Fig. 4(a).

The temperature profiles measured in an experiment on a Ti–6Al–4V specimen at an impact velocity of 47.3 ms^{-1} are shown in Figs 10 and 11. The lowest temperature that can be measured by the detectors for this material is approximately 360 K. Similar to the results in Figs 8 and 9, temperatures inside the shear band reach a maximum of 680 K (407°C) in approximately 60–70 μs. There appear to be differences in the temperature profiles of the C-300 steel and those of the titanium alloy. The greatest of these differences occurs in the maximum temperatures observed. Temperatures are significantly higher in C-300 than they are in Ti–6Al–4V. The much lower temperatures for Ti–6Al–4V are consistent with the ductile failure morphology in Fig. 4(b) which shows no smearing of the voids.
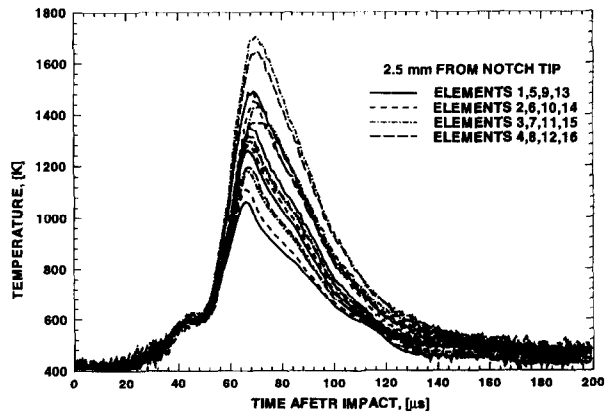
Figure 12 is a summary of the maximum temperatures observed inside the shear bands at different impact velocities for these two materials as a function of the
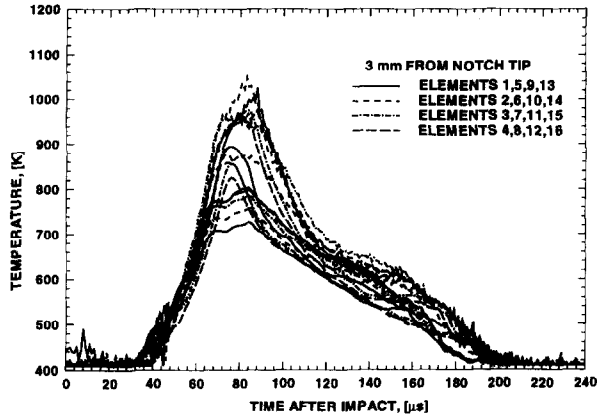
(a) C-300 #10, V_0=23.4 ms^{-1}
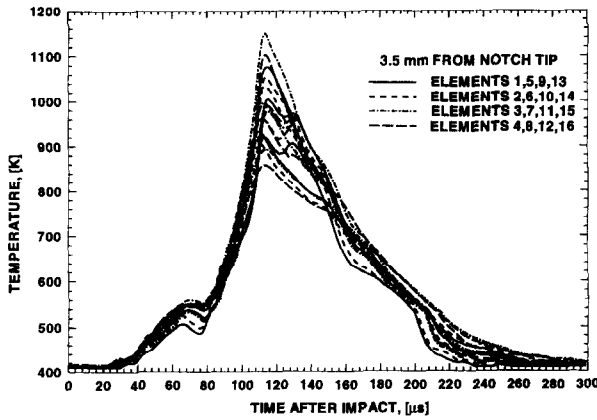
(b) C-300 #08, V_0=33 ms^{-1}

(c) C-300 #02, V_0=42.8 ms^{-1}

Fig. 8. Temperature profiles around propagating shear bands; C-300 steel (a) C-300, $V_0 = 23.4$ ms^{-1}; (b) C-300, $V_0 = 33$ ms^{-1}; (c) C-300, $V_0 = 42.8$ ms^{-1}.
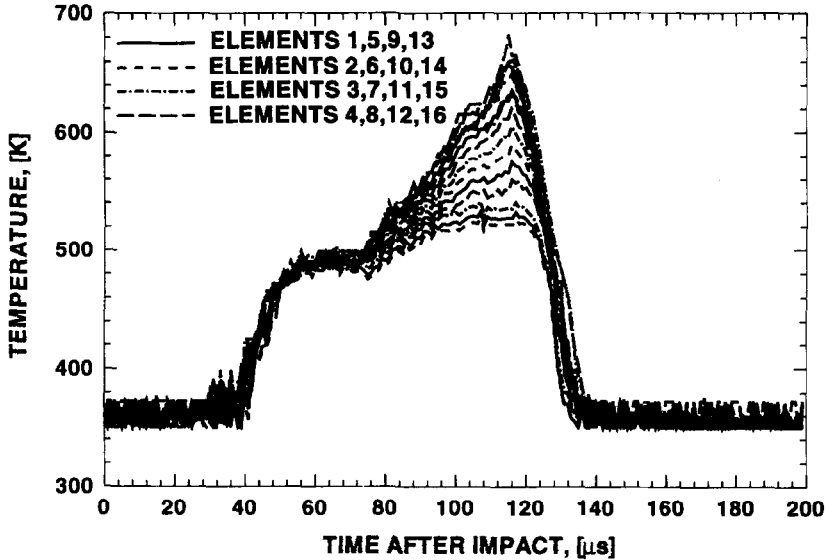
Fig. 10. Temperature profiles around a propagating shear band; Ti–6Al–4V, $V_0 = 47.3$ ms^{-1}.
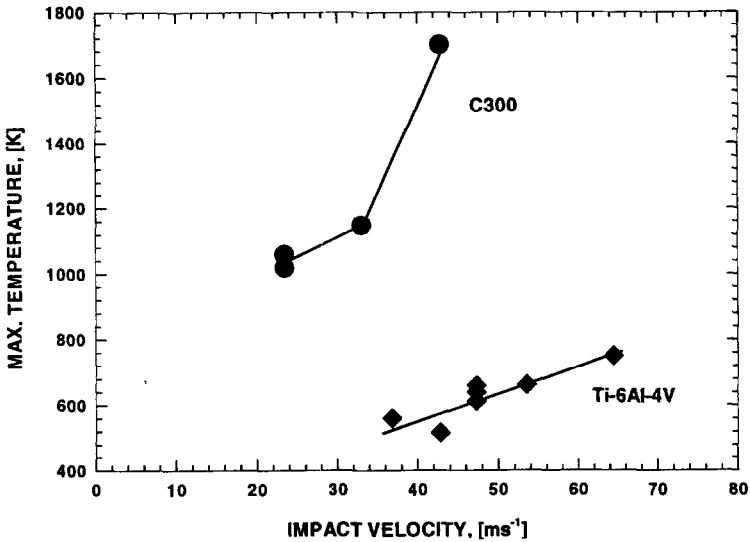

Fig. 12. Maximum temperature as a function of impact velocity.

projectile velocity. While the maximum temperatures increase monotonically with the impact velocity for both materials, the maximum temperature values are significantly lower in the titanium alloy than in the steel for the same impact velocity. For C-300, the highest temperature observed approaches 1700 K (1400°C) or 90% of its melting point. On the other hand, the highest temperature observed for Ti–6Al–4V is 750 K (450°C) which occurs at a much higher impact velocity (64.5 ms^{-1}). This is also

consistent with the observation that shear bands in the titanium alloy are more diffuse or wider and more difficult to form than the bands in the C-300 steel. Many factors, such as the fraction of plastic work converted to heat, can greatly influence the temperatures attained inside the shear bands. Mason *et al.* (1994b) found that the fraction of plastic work converted to heat changes differently in these two materials as deformation progresses. For steels, this fraction remains close to 0.85–0.9 for plastic strains up to 0.3. For Ti–6Al–4V, this fraction decreases when plastic strain exceeds 0.05. This decrease contributes to the reduction of thermo-mechanical heating available in Ti–6Al–4V. The speed at which a shear band propagates also influences the temperature inside it. Higher speeds correspond to higher rates of deformation and therefore translate into higher temperatures. As will be seen in Section 5, shear bands propagate at much higher speeds in C-300 than in Ti–6Al–4V. This difference in propagation speed also partly explains the distinct temperature levels observed in these two materials. Finally, differences in mass density and specific heat may also contribute to the different behaviors.

The temperatures observed here for the C-300 steel are substantially higher than those previously reported by Duffy and Chi (1992) for steels in dynamic torsion experiments. In addition to differences in material properties, other factors may also contribute to the different temperature levels. In the torsional experiment of Duffy and Chi, there is no hydrostatic pressure. Therefore, material fracture is not inhibited by a superimposed hydrostatic pressure. Earlier fracture limits temperature increase by eliminating further heat generation through continued deformation. In the current experiment, the material within the extending band is also subjected to a superimposed pressure due to the impact loading which retards eventual fracture along the shear band plane. The prolonged deformation contributes to higher temperature increases inside the shear band. Because of the same reason, temperatures inside propagating shear bands may reach higher levels than temperatures at the tip of propagating cracks, see Zehnder and Rosakis (1991, 1992) and Zehnder and Kallivayalil (1991). The magnitude, the spatial variation and the time scale of the temperature changes shown above clearly demonstrate the dynamic nature of the phenomenon, the extent of thermal softening due to such temperature rises and the need to study it in real time.

Figure 13(a) shows temperature profiles along a shear band path in a C-300 specimen obtained by using the configuration of Fig. 7(c). The impact velocity is 29.7 ms^{-1}. The profiles indicate small time delays in temperature rises at different points along the path where the detector elements are located. To facilitate the visualization of the small time delays, temperature histories for the two end points of the detector array separated by 1.5 mm along the shear band path are shown in Fig. 13(b). The delay is approximately 2–3 μs in the intitial part of the temperature profiles. Temperature at the point closer to the initial notch tip (Element 1) begins to increase earlier than the temperature at the point farthest away from the tip (Element 16). This is due to the fact that the shear band initiates from the notch tip and propagates toward the detector elements. This delay corresponds to an initial shear band speed of 500–600 ms^{-1}, depending on how the time delay is measured. This estimate is in agreement with the result of optical measurement of the shear band propagation speed corresponding to early times after initiation, as discussed in the next section of
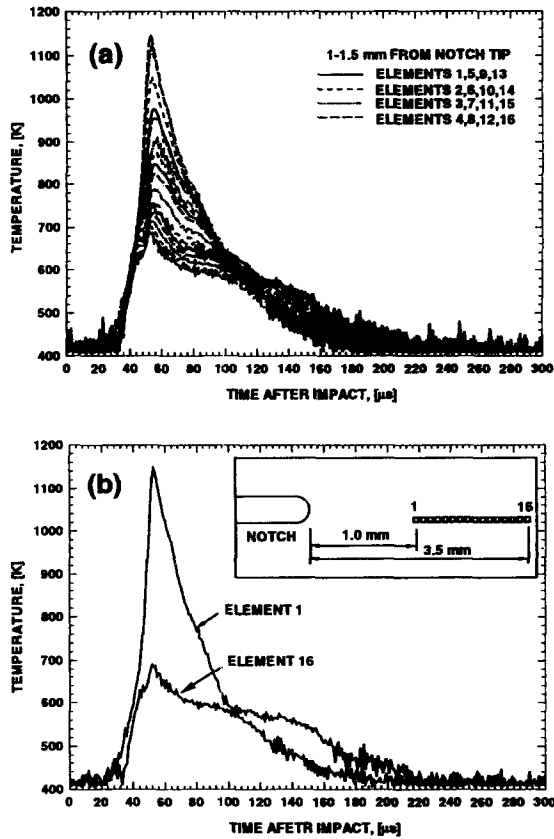
Fig. 13. Temperature profiles at different distances from the notch tip, C-300 $V_0 = 29.7$ ms^{-1}.

this paper. Temperature profiles along a shear band path in a Ti–6Al–4V specimen are shown in Fig. 14. The impact velocity is 64.5 ms^{-1}. Clearly, the time delays between the profiles at different distances from the initial notch tip are higher than those observed in Fig. 13. The delay between the first point (Element 1) and the last point (Element 16) is approximately 15–16 μs. This delay corresponds to a shear band speed of approximately 100 ms^{-1}, which is significantly lower than the speed observed for the C-300 specimen of Fig. 13. Note also that the impact velocity for the titanium alloy specimen is much higher than that of the C-300 specimen.

5. SHEAR BAND VELOCITY HISTORIES

The different thermal behaviors of the two materials are also corroborated by the shear band lengths measured after the experiments, as shown in Fig. 15. For the steel, the band extends from zero to a maximum length of 50 mm (which is the size of the ligament) in an impact velocity range of 19–29 ms^{-1}. For the titanium alloy, the band extension is less than 7–8 mm for impact velocities up to 64.5 ms^{-1}. The dramatically
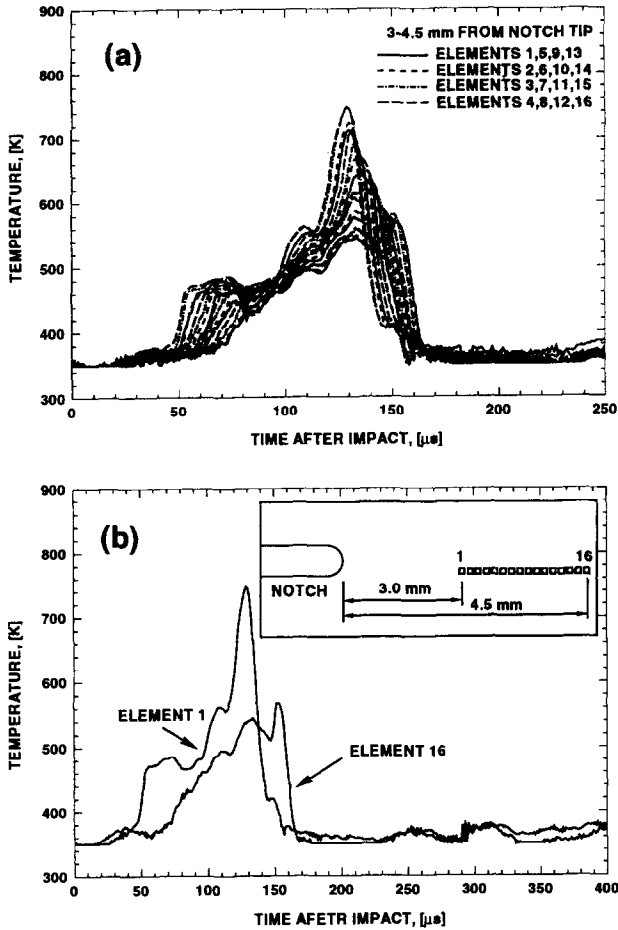
Fig. 14. Temperature profiles at different distances from the notch tip, Ti–6Al–4V, $V_0 = 64.5$ ms^{-1}.

different distances of gross shear band extension is another direct indication that shear bands propagate at very different speeds in these two materials. Higher speeds are associated with higher rates of deformation inside the bands and, therefore, produce higher temperatures. Differences in the mechanical properties also play a role in causing the distinct thermal and propagation behaviors of these two materials. The lower impedance of Ti–6Al–4V corresponds to lower input stresses under the same impact velocity compared with C-300, thus reducing the intensity of the stress and deformation fields at the notch tip. Next, attention is focused on the propagation of shear bands in the C-300 steel. This material is chosen since it shows longer and faster shear band propagation. In addition, the relatively smaller out-of-plane deformation for C-300 reduces the aperture effect that makes it difficult to record the near fields around the propagating shear bands with the high speed camera system.

    Figure 16 shows a selected sequence (6 out of a total of 80) of images of the propagating shear band during an experiment with an impact velocity of 25 ms^{-1}.
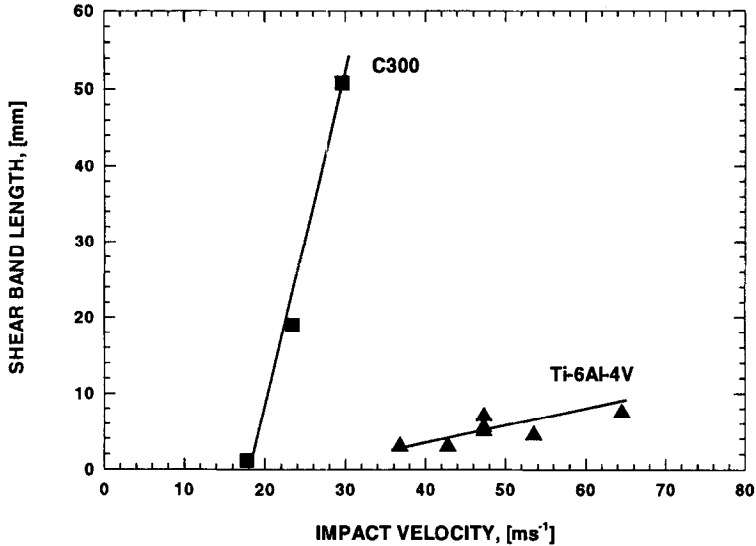
Fig. 15. Maximum shear band length as a function of impact velocity.

These images are recorded with the optical setup and the high speed camera illustrated on the right hand side of Fig. 6. In the pictures, the diameter of the circular field of view is 50.4 mm. The grid of parallel lines perpendicular to the shear band is deposited on the specimen to enhance visualization of the shear band propagation. The grid has a pitch of approximately 0.74 mm. The initial notch is on the left side of the photographs. The impact takes place on the lower side of the notch toward the right. Areas very close to the shear band are not visible due to the aperture effect in the imaging system. The formation of the dark strip surrounding the shear band is a result of the relatively large surface rotation (or out-of-plane displacement gradient) due to high gradients of deformation inside the shear band. When coherent light is used, such an effect can not be totally eliminated because of the finite aperture size in the camera system. Since the size of the dark strip (or shadow) is relatively small compared with the distance of propagation and since the changes in its width are very small, relatively accurate information concerning the shear band initiation time, shear band path and shear band length, can be obtained from these images. In Fig. 16, the initiation occurs between the first and the second frames (at 14 and 35 μs after impact, respectively). From images recorded between these two frames the initiation is found to be at approximately 23 μs. It can be seen that the shear band arrests at approximately 60 μs after impact. This coincides with the end of the in-plane shear loading at the tip of the shear band generated by the impact, as shown by the numerical simulations of Zhou et al. (1995) in Part II of this investigation. After 60 μs, the shear band is stationary relative to the specimen and no apparent propagation is identifiable from the images. At approximately 140 μs, an upturn in the path of propagation toward a direction approximately 35° away from the original direction of propagation is seen in the recorded images. This upturn indicates the emergence of an opening mode of loading at the tip of the arrested shear band. It is the occurrence of this tensile mode
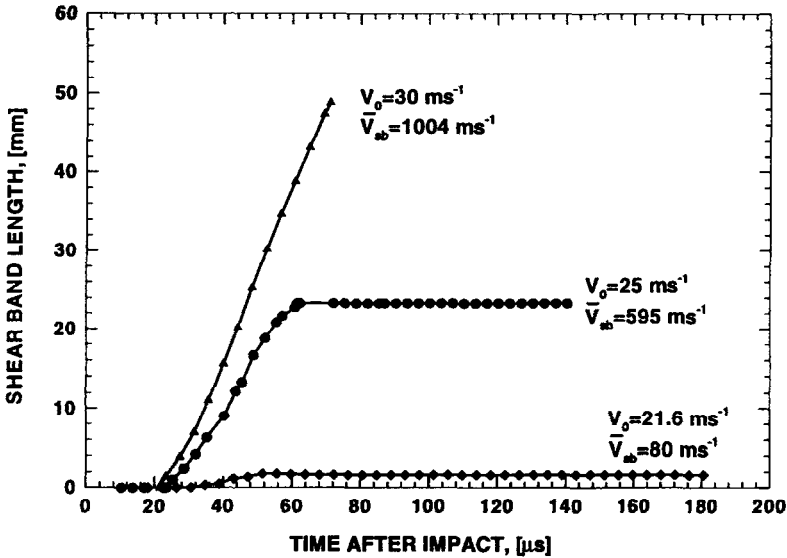
Fig. 18. Shear band length histories for C-300 at different impact velocities.

of loading and an associated increase in tensile stresses that cause fracture to occur as illustrated in Figs 1 and 3, see Zhou *et al.* (1996). In the actual experiment, the angles at which the crack forms vary around $30°$. The exact value of this angle may be partly influenced by the effects of the different lengths and speeds of shear band propagation on the loading conditions in the specimens. The grid of lines in the images also provide information about the shear deformation around the shear band. The misalignment between lines above and below the band in the frames for up to 65 μs clearly show shear deformation during propagation. This misalignment no longer exists in the images between 90 and 140 μs. Instead, a slight misalignment in the opposite direction can be seen in the frame at 140 μs. This is not entirely caused by elastic recovery. Rather, it is due to a reversed shear loading that existed at the shear band region after the shear band arrests. This shear, which is in a direction opposite to the direction of initial shear, is a result of the stress wave reverberations in the specimen, as demonstrated by the numerical calculations in Part II of this investigation.

Figure 17 shows another sequence of images of a propagating shear band in an experiment with an impact velocity of 29.7 ms^{-1}. Due to the higher impact velocity, the initiation occurs slightly earlier, at approximately 22 μs after impact. Also, the propagation is faster. By approximately 65 μs the shear band has propagated through the whole ligament (50.4 mm) of the specimen. Consequently, the transition of failure mode indicated in the last frame of Fig. 16 could not occur due to total specimen separation.

Figure 18 summarizes the histories of shear band length measured from the images obtained at three impact velocities. The curves show a dramatic increase in shear band length with impact velocity. For these impact conditions, shear band initiation occurs between 20 and 28 μs after impact. It can be clearly seen that shear band
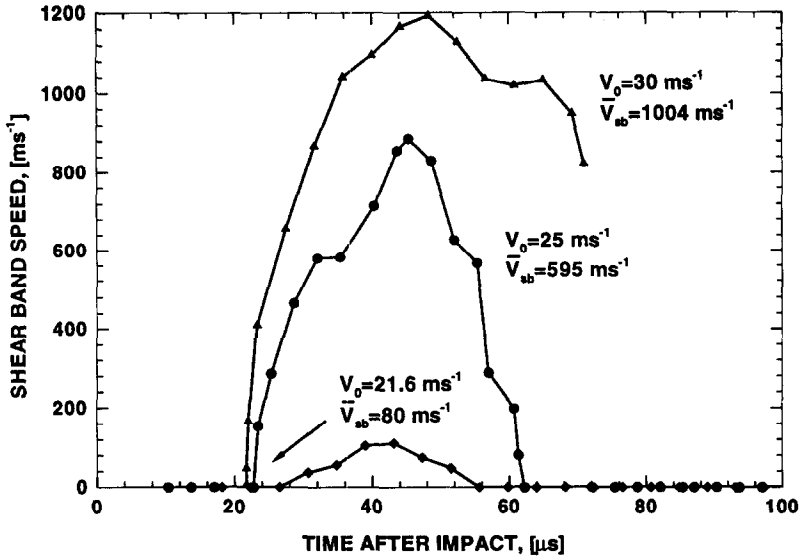
Fig. 19. Shear band speed histories for C-300 at different impact velocities.

extension and thus the loading that is responsible for the initiation and propagation end at about 60–65 μs.

The shear band speed histories in Fig. 19 are obtained by differentiating the length records in Fig. 18. The shapes of curves indicate that the shear bands do not propagate at constant speeds. The speed is lower initially and reaches a maximum for each of the impact velocities. Note that the maximum speeds and the average speeds (total band length divided by the time duration of extension) are close for each of these impact conditions. The records exhibit a region of very high shear band acceleration, a plateau of approximately steady speed and a region of very high deceleration. The maximum acceleration and deceleration are of the order of 10^8 ms^{-2}. The curves also show a dramatic increase in the shear band speed over the impact velocity range 20–30 ms^{-1}. The highest speed observed is close to 1200 ms^{-1}. This value is approximately 38% of the shear wave speed of the specimen material. The dependence of the shear band speed on impact velocity is shown in Fig. 20. Both the maximum speed and the average speed measured for each impact velocity are shown. This figure clearly demonstrates the quick increase of shear band speed over a short region of impact velocity. First, it can be seen that the impact velocity required to initiate a shear band is approximately 20 ms^{-1}. Below this value, no shear band is observed. The rate of increase is lower at higher impact velocities. The shape of the curves does not indicate a saturation of shear band speed with further increase in impact speed. Data presented in Fig. 20 strongly suggest the possibility of observing higher values for the speed of shear band propagation. In actual experiments discussed here, the observation of such higher speeds is limited by the occurrence of ductile failure at the projectile–specimen impact site when the impact velocity is increased beyond 45 ms^{-1}. Failure at the impact site not only reduces the magnitude but also changes the well-characterized nature of the asymmetric loading applied to the notch tip. This is the first time such
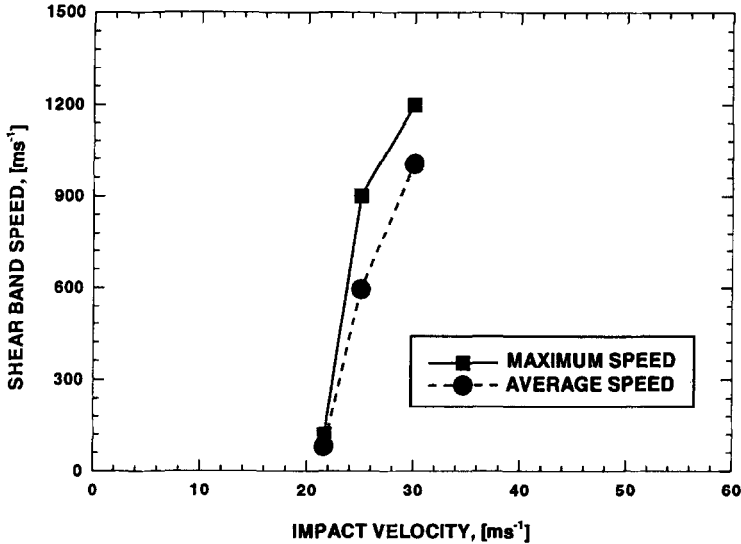
Fig. 20. Maximum and average shear band speeds as functions of impact velocity for C-300 steel.

high shear band speeds have been reported in the open literature. The observed speeds are higher, by a factor of two, than those measured by Marchand and Duffy (1988) in a torsional Kolsky bar configuration. In a similar impact configuration as the one used here, Mason et al. (1994a) reported initial band speeds of approximately 320 ms^{-1} at early times after initiation for an impact velocity of 38 ms^{-1}. This number is consistent with the results in Fig. 19.

6. CONCLUSIONS

Dynamic failure in notched plates is studied experimentally for specimens of C-300 and Ti–6Al–4V. Controlled shear band initiation and propagation are obtained by using the stress and deformation fields at the tip of an asymmetrically impact-loaded notch as a trigger. There exists a transition in the mode of failure from ductile shear banding (shear mode) to brittle cracking (opening mode) at intermediate impact velocities for C-300. Such a transition is not observed for the titanium alloy. While the transition is induced by tensile loading that occurs as a result of stress wave evolutions in the specimens after the arrest of the shear band, the absence of this transition in Ti–6Al–4V specimens suggests that it is also related to material properties. Experimental results show that these two materials exhibit distinct resistances to failure under the conditions considered. C-300 is more susceptible to failure by both propagating shear bands and propagating cracks than Ti–6Al–4V.

Temperature fields around propagating shear bands are studied experimentally. Measurements revealed the structure of the fields and indicated distinct temperature rises for C-300 and for Ti–6Al–4V. For C-300, the temperature profiles show significant heating in a narrow strip approximately 200–300 μm in width. Shear bands

are more diffuse in the titanium alloy. The maximum temperatures measured inside the shear bands are found to increase with the impact velocity for both materials. While the temperature approaches 1400°C (or approximately 90% of its melting point) for C-300 as the impact velocity increases to 43 ms^{-1}, the maximum temperature observed in Ti–6Al–4V is only 450°C as the impact velocity increases to 64.5 ms^{-1}. This marked difference is corroborated by the levels of shear band speeds in the two materials, indicating a stronger resistance to shear banding by the titanium alloy than by the steel under the conditions of the experiments.

The propagation of shear bands is also studied by high speed photography. There is a dramatic increase in the speed of shear bands over a short range of impact velocity for C-300. The maximum shear band speed observed in C-300 steel is 1200 ms^{-1} or approximately 40% of the shear wave speed of the material. The maximum speed and the average speed of shear band propagation are close to each other and show a strong dependence on the impact velocity. The high speed camera images capture the complete sequence of events including initiation and growth of the shear band. In cases involving shear band arrest, the high speed photography also demonstrates the transition in the mode of failure from shear banding to cracking.

ACKNOWLEDGEMENTS

REFERENCES

Bai, Y. L. (1981) A criterion for thermo-plastic shear instability. *Proc. Int. Conf. on Metallurgical Effects of High-Strain-Rates Deformation and Fabrication*, Albuquerque, NM, pp. 277–283. Plenum, NY.

Bai, Y. L. (1982) Thermo-plastic instability in simple shear. *J. Mech. Phys. Solids* **30**, 195–207.

Batra, R. C. and Kim, C. H. (1992) Analysis of shear banding in twelve materials. *Int. J. Plasticity* **8**, 425–452.

Clifton, R. J. (1980) Adiabatic shear banding. *Material Response to Ultra-High Loading Rates*, NMAB-356, Ch. 8. National Materials Advisory Board (NRC), Washington, DC.

Duffy, J. and Chi, Y. C. (1992) On the measurement of local strain and temperature during the formation of adiabatic shear bands. *Mater. Sci. Engng* **A157**, 195–210.

Freund, L. B., Wu, F. H. and Toulios, M. (1985) *Proc. Considere Memorial Symposium*, p. 125. Presse de l'Ecole Nationale des Pontes et Chaussees, Paris.

Gioia, G. and Ortiz, M. (1996) The two-dimensional structure of dynamic shear bands in thermoviscoplastic solids. *J. Mech. Phys. Solids* **44**, 251–292.

Giovanola, J. H. (1988), Adiabatic shear banding under pure shear loading, part I: Direct observation of strain localization and energy dissipation measurements, Part II: Fractographic and metallurgraphic observations. *Mech. Mater.* 59–87.

Grady, D. E. (1992) Properties of an adiabatic shear-band process zone. *J. Mech. Phys. Solids* **40**, 1197–1215.

Kalthoff, J. F. (1987) Shadow optical analysis of dynamic shear fracture. *SPIE, Photomechanics and Speckle Metrology* **814**, 531–538.

Kalthoff, J. F. and Wrinkler, S. (1987) Failure mode transition at high rates of shear loading. *Impact Loading and Dynamic Behavior of Materials* (ed. C. Y. Chiem, H.-D. Kunze and L. W. Meyer), Vol. 1, pp. 185–195.

Klemm, W., Winkler, S. and Reisacher, E. (1989) The energy consumption by dynamic shear fracture, dynamic fracture. *Proc. OJI Int. Seminar on Dynamic Fracture*, 1–4 August, pp. 77–92.

Lee, Y. J. and Freund, L. B. (1990) Fracture initiation due to asymmetric impact loading of an edge cracked plate. *Trans. ASME* **57**, 104–111.

Marchand, A. and Duffy, J. (1988) An experimental study of the formation process of adiabatic shear bands in a structural steel. *J. Mech. Phys. Solids* **36**, 251–283.

Mason, J. J., Rosakis, A. J. and Ravichandran, G. (1994a) Full field measurements of the dynamic deformation field around a growing adiabatic shear band at the tip of a dynamically loaded crack or notch. *J. Mech. Phys. Solids* **42**, 1679–1697.

Mason, J. J., Rosakis, A. J. and Ravichandran, G. (1994b) On the strain and strain-rate dependence of the fraction of plastic work converted to heat: An experimental study using high speed infrared detectors and the Kolsky bar. *Mech. Mater.* **17**, 135–145.

Merzer, A. M. (1982) Modelling of adiabatic shear band development from small imperfections. *J. Mech. Phys. Solids* **30**, 323–338.

Molinari, A. and Clifton, R. J. (1987) Analytical characterization of shear localization in thermoviscoplastic materials. *Trans. ASME, J. Appl. Mech.* **54**, 806–812.

Needleman, A. (1989) Dynamic shear band development in plane strain. *J. Appl. Mech.* **56**, 1–9.

Needleman, A. and Tvergaard, V. (1994) Analysis of brittle-ductile transition under dynamic shear loading. *Symp. Dynamic Failure Mechanics of Modern Materials*, Caltech, Pasadena, CA, 3–5 February, 1994.

Recht, R. F. (1964) Catastrophic thermoplastic shear. *J. Appl. Mech.* **86**, 189–193.

Rogers, H. C. (1979) Adiabatic plastic deformation. *Ann. Rev. Mater. Sci.* **9**, 283–311.

Rogers, H. C. and Shastry, C. V. (1981) Material factors in adiabatic shearing in steels. *Shock Waves and High Strain-rate Phenomena* (ed. M. A. Meyers and L. E. Murr), Ch. 18, pp. 285–298. Plenum Press.

Shawki, T. G. (1992) The phenomenon of shear strain localization in dynamic viscoplasticity. *Appl. Mech. Rev.* **45**, s46–s60.

Shawki, T. G. and Clifton, R. J. (1989) Shear band formation in thermal viscoplastic materials. *Mech. Mater.* **8**, 13–43.

Wright, T. W. and Walter, J. W. (1987) On stress collapse in adiabatic shear bands. *J. Mech. Phys. Solids* **35**, 701–720.

Zehnder, A. T. and Kallivayalil, J. A. (1991) Temperature rise due to dynamic crack growth in beta-C titanium. *Speckle Techniques, Birefringence Methods, and Applications to Solid Mechanics, SPIE* **1554A**, p. 48.

Zehnder, A. T. and Rosakis, A. J. (1991) On the temperature distribution at the vicinity of dynamically propagating cracks in 4340 steel. *J. Mech. Phys. Solids* **39**, 385–415.

Zehnder, A. T. and Rosakis, A. J. (1992) Temperature rise at the tip of dynamically propagating cracks: measurements using high-speed infrared detectors. *Experimental Techniques in Fracture* (ed. J. S. Epstein), pp. 125–169. VCH Publishers.

Zbib, H. M. and Aifantis, E. C. (1992) On the gradient-dependent theory of plasticity and shear banding. *Acta Mech.* **92**, 209–255.

Zhou, M., Needleman, A. and Clifton, R. J. (1994) Finite element simulations of dynamic shear localization in plate impact. *J. Mech. Phys. Solids* **42**, 423–458.

Zhou, M., Ravichandran, G. and Rosakis, A. J. (1996) Dynamically propagating shear bands in prenotched plates: II—Finite element simulations. *J. Mech. Phys. Solids* **44**, 1007–1032.

Zurek, A. K. (1994) The study of adiabatic shear band instability in a pearlitic 4340 steel using a dynamic punch test. *Metall. Mater. Trans. A* **25A**, 2483–2489.